AD_____

Award Number: W81XWH-07-1-0457

TITLE: Magnetic Nanoparticle-Based Imaging of RNA Transcripts in Breast Cancer Cells

PRINCIPAL INVESTIGATOR: Andrew Tsourkas

CONTRACTING ORGANIZATION: Trusteees of the University of Pennsylvania
Philadelphia, PA 19104-6205

REPORT DATE: June 2008

TYPE OF REPORT: Annual

PREPARED FOR: U.S. Army Medical Research and Materiel Command
Fort Detrick, Maryland 21702-5012

DISTRIBUTION STATEMENT: Approved for Public Release;
Distribution Unlimited

REPORT DOCUMENTATION PAGE

Form Approved
OMB No. 0704-0188

1. REPORT DATE	2. REPORT TYPE	3. DATES COVERED
30-06-2008	Annual	1 JUN 2007 - 31 MAY 2008

4. TITLE AND SUBTITLE

Magnetic Nanoparticle-Based Imaging of RNA Transcripts in Breast Cancer Cells

5a. CONTRACT NUMBER

5b. GRANT NUMBER
W81XWH-07-1-0457

5c. PROGRAM ELEMENT NUMBER

6. AUTHOR(S)
Andrew Tsourkas

Email: atsourk@seas.upenn.edu

5d. PROJECT NUMBER

5e. TASK NUMBER

5f. WORK UNIT NUMBER

7. PERFORMING ORGANIZATION NAME(S) AND ADDRESS(ES)

Trustees of the University of Pennsylvania
Philadelphia, PA 19104-6205

8. PERFORMING ORGANIZATION REPORT NUMBER

9. SPONSORING / MONITORING AGENCY NAME(S) AND ADDRESS(ES)
U.S. Army Medical Research and Materiel Command
Fort Detrick, Maryland 21702-5012

10. SPONSOR/MONITOR'S ACRONYM(S)

11. SPONSOR/MONITOR'S REPORT NUMBER(S)

12. DISTRIBUTION / AVAILABILITY STATEMENT
Approved for Public Release; Distribution Unlimited

13. SUPPLEMENTARY NOTES

14. ABSTRACT

We have developed a novel approach to detect RNA transcripts via magnetic resonance by taking advantage of the decrease in the spin-spin (i.e. T2) relaxation time that results from the self-assembly of superparamagnetic iron oxide nanoparticles (NPs). Specifically, two unique NP-oligonucleotide (ON) conjugates were designed to recognize adjacent sites on nucleic acid targets (Figure 1). Thus, upon hybridization to complementary targets the NP-ON conjugate pairs were brought into close proximity, which resulted in a detectable reduction in the T2 relaxation time. This mechanism of switching from a high T2-relaxation time to a low T2-relaxation time is generally referred to as magnetic relaxation switching (MRSw). In the presence of target nucleic acids, we measured as much as a 40% decrease in T2 signal due to aggregate formation, with reliable detection of target at levels as low as 10 pmoles. We have also prepared NPs with sizes ranging from ~20 nm to 1 um and identified that positively charged NPs <200 nm are taken up by cells much more effectively than larger NPs. Therefore, we plan to use NPs in this size range when attempting to detect RNA in cells.

15. SUBJECT TERMS
Iron oxide nanoparticles, RNA, detection, sensor

16. SECURITY CLASSIFICATION OF:			17. LIMITATION OF ABSTRACT	18. NUMBER OF PAGES	19a. NAME OF RESPONSIBLE PERSON
a. REPORT	b. ABSTRACT	c. THIS PAGE			USAMRMC
U	U	U	UU	17	19b. TELEPHONE NUMBER *(include area code)*

Table of Contents

INTRODUCTION:

The goal of the proposed research is to develop a novel approach to image mRNA transcripts via magnetic resonance (MR). Specifically, nucleic acids will be detected by taking advantage of the change in MR contrast that results when two or more superparamagnetic nanoparticles (NPs) are brought into close proximity. The NPs are brought together by designing them such that they bind to adjacent sites on mRNAs that are highly over-expressed in breast cancer cells. The first specific aim of this project involves the synthesis and optimization of magnetic nanoparticle-oligonucleotide (NP-ON) conjugates. In particular, we proposed to synthesize NPs of differing size, magnetic properties, and surface modifications. We then proposed to evaluate which NP configuration allows for the highest sensitivity of RNA detection. Our second specific aim is focused on efficiently delivering NPs into the cytoplasm of breast cancer cells, where they will have access to intracellular mRNA. Of particular interest is the rate and extent of internalization of NPs of varying size and charge. Also, we are interested in the localization of internalized NPs and will explore various endosomal disruption agents to facilitate cytoplasmic delivery. The third aim involves testing whether we can correlate a change in MR contrast to the level of target mRNA in cell lysate and in living breast cancer cells.

BODY:

Task 1. To synthesize and optimize magnetic nanoparticle-oligonucleotide (NP-ON) conjugates for detecting nucleic acid targets (Years 1 – 3)

a. Synthesize dextran-coated superparamagnetic nanoparticles with amine or carboxyl groups available for conjugation. (Years 1 - 3)

To date we have achieved the ability to synthesize NPs with tightly controlled physical, magnetic and chemical characteristics with a high degree of reliability. Detailed protocols outlining the synthetic procedures for aminated nanoparticles can be found in the appended publication (Thorek et al., 2008). We have also been able to successfully prepare carboxylated NPs by reacting the aminated nanoparticles with succinic anhydride. Conversion of the amine groups to carboxyl groups was validated by running the NPs on a 1% agarose gel. The carboxylated (i.e. negatively charged) NPs migrated towards the cathode, whereas the aminated NPs migrated towards the anode.

b. Determine iron-oxide core size, hydrodynamic radius, and relaxivities of the magnetic nanoparticles. (Years 1 - 3)

NPs have been synthesized with hydrodynamic diameters ranging from ~20 nm to ~120 nm. Several examples of NPs within this size range are presented in the appended publication (Thorek el al, 2008). Interestingly, all of the NPs synthesized had iron oxide cores of similar size (~6 nm); however, the larger NPs possessed multiple cores. Therefore, the larger NPs had a larger "effective" core size. The number of cores ranged from ~1 for the NPs with a ~20 nm hydrodynamic diameter to ~11 for NPs with a hydrodynamic diameter of ~110 nm. The R2 relaxivity increased directly with the NP "effective" core size. For example, a 33 nm NP exhibited an R2 of 71 $mM^{-1}s^{-1}$, while a 107 nm NP exhibited an R2 of 381 $mM^{-1}s^{-1}$. The R1

values decreased with increasing hydrodynamic diameter, going from 13.56 $mM^{-1}s^{-1}$ for the 33 nm NPs to 7.24 $mM^{-1}s^{-1}$ for the 107 nm NPs.

Although the dextran-coated iron oxide NPs were synthesized as proposed, we felt that one limiting feature for comparative studies was the large distribution in size that was observed for each batch of NPs prepared. In other words, although we could control the mean size of the NPs, there was still a relatively large distribution in both the hydrodynamic diameter and the number of cores. Therefore, we have begun synthesizing iron oxide nanoparticles via thermal decomposition (Park et al, 2004). This synthetic approach allows for the synthesis of NPs with single iron oxide cores of relatively monodisperse size. The size can also be controlled by varying the synthetic conditions. Thus far, we have made NPs with an iron oxide core diameter of ~5nm using this method (Figure 1). We are now preparing to make NPs with larger cores as well. To make these NPs water-soluble we have seeded a gold coating onto the NP surface. An example transmission electron microscopy image is shown in Figure 1. We believe that this will also facilitate ON conjugation as discussed below. Currently, we are also working to make the gold coating as thin as possible.

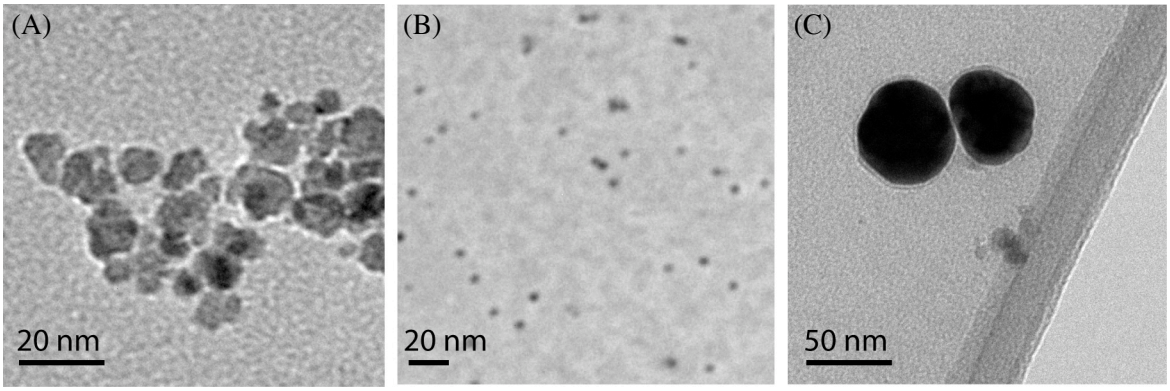

Figure 1. Transmission electron microscope images of iron oxide nanoparticles. (A) Dextran-coated iron oxide nanoparticles. TEM images show that the iron oxide cores are heterogeneous in size. (B) Iron oxide nanoparticles prepared by thermal decomposition. TEM images show relatively uniform size distribution of iron oxide cores. (C) TEM image of gold-coated iron oxide nanoparticles.

c. Use chemical cross-linkers to attach oligonucleotides to the magnetic nanoparticles. Oligonucleotides will be synthesized with a photocleavable linkage. (Years 1 - 3)

We have explored two different approaches for attaching ONs to the nanoparticles. Specifically, the approaches that we have developed include (1) reacting the ON with disuccinimidyl suberate (DSS), precipitating the ON in acetone, and resuspending the ON pellet in aminated NPs and (2) reacting carboxylated NPs with EDC and sulfo-NHS, precipitating the NPs in isopropanol, and resuspending in aminated ONs. The number of ONs per NP was easily determined since we labeled each oligonucleotide with a fluorescent dye that can be quantified via absorbance measurements. The number of ONs per NP is typically in the range of 2 to 10 depending on the nanoparticle synthesis protocol. When a particular batch of NPs was used, the number of ONs per nanoparticle was relatively consistent for each trial. It should be noted that initially we were preparing ONs with photocleavable linkages, but due to the additional cost and lower yields of

this ON synthesis we have decided to only add the photocleavable linkages after NP optimization is complete. Since, our optimization studies can be conducted in a controlled environment, i.e. in test tubes, photocleavable linkages are not necessary at this stage. They are only necessary for live cell studies.

One of the limitations of our current conjugation schemes is it is somewhat difficult to control the number of ONs per NP for each particular NP batch. Moreover, because chemical cross-linkers are quickly hydrolyzed in aqueous solvents it is often necessary to use a large quantity of ONs for each synthesis (i.e large molar excess). To address this problem we decided to explore synthesizing gold coated iron oxide nanoparticles. It was hypothesized that gold coated iron oxide nanoparticles could facilitate conjugation chemistry since thiolated oligonucleotides could be readily conjugated to the gold coating. Thus far, we have successfully synthesized gold-NPs (Figure 1) and are just begun testing DNA conjugations.

d. Perform hybridization assays with NP-ON conjugates in the presence of varying amounts of nucleic acid targets and record T2 relaxation times before and after UV exposure. Analogous studies will be performed with a mutant (not perfectly complementary) target to serve as a negative control. Targets with a varying number of binding sites and varying spacing between binding sites will also be tested. (Months 4 - 12)

The lower detection limit for nucleic acid detection was determined by serially diluting samples of oligonucleotide targets (1 μM to 1 aM) and mixing them with pairs of NP-ONs that hybridize to adjacent sites on the target DNA. Using 33 nm NP-ONs with an R2 of 71 $(mMsec)^{-1}$ and ~3 ONs per NP, we have found that we can detect as little as 10 pmoles of target (Figure 2). Higher target concentrations produced as much as a 41% change in T2 signal (38 ms). Furthermore, the signal reduction was not seen when similar concentrations of a non-specific target was used. We have also tested whether the spacing between NPs on the oligonucleotides target influences our lower detection limit. Specifically, we have tested NP-ON probes that bind to DNA targets with no space between the hybridized NP-ONs and with a spacing of 6 bases between the hybridized NP-ON. We did not observed any statistical difference in the T2-relaxation times measured when NP-ONs were incubated with these two targets. This is most likely because this single stranded domain most likely forms a random coil and thus does not have a significant impact on the distance between NP-ONs. We plan to test much larger spacer lengths in the near future.

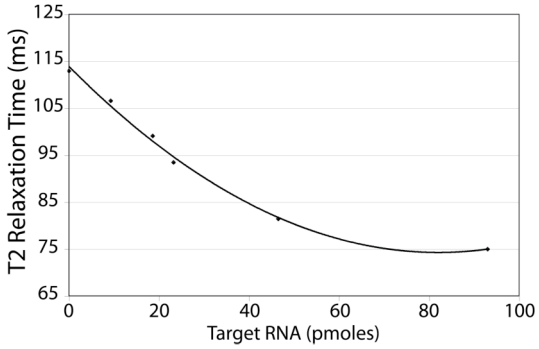

Figure 2. Detection of RNA via Magnetic Relaxation Switching. Binding of NP-ONs to adjacent sites on nucleic acid targets led to a dramatic decrease in the T2 relaxation time. The extent of change in the T2 relaxation time correlated directly with target concentration with a maximum reduction (39.4%) occurring at ~95 pmoles.

Task 2. To delivery NP-ON conjugates to the cytoplasm of MCF-7 breast cancer cells

a. Synthesize nanoparticles that are linked to both oligonucleotides and cell internalizing peptides (pNP-ONs). (Years 2 - 3)

We have not yet synthesized NPs with cell internalizing peptides, but we have observed that even just aminated NPs are efficiently internalized into cells. This has allowed us to evaluate the cellular uptake of NPs over a continuum of NP sizes ranging from 33 nm to nearly 1.5 um without the added complexity of conjugating peptides. Our results can be found in the appended publication (Thorek et al., 2008). In short, we found that NPs < 200 nm are taken up more efficiently than larger NPs. Therefore, we will focus on NPs within this size range for our RNA detection studies.

b. Measure the rate and extent of pNP-ON internalization in MCF-7 breast cancer cells. NP-ONs with no internalizing peptide will be used as a control (Months 12 - 18).

We have analyzed the rate and extent of NP uptake in T cells (Thorek, 2008), but have not yet conducted these studies in MCF-7 cells, although we do expect to observe similar results. Briefly, we found that for T cells internalization of NPs < 200 nm in diameter can be saturated within ~ 1hr when NPs are at a concentration of ~ 50 ug/mL.

c. Image the localization of pNP-ONs in the cell cytoplasm (Months 18 - 24)

These studies have not yet commenced.

d. Test various endosomal disruption agents to examine whether they can facilitate the delivery of pNP-ONs to the cytoplasm of cells (Months 24 - 30).

These studies have not yet commenced.

Task 3. To detect c-myc expression in breast cancer cells (Months 4-12)

a. Incubate NP-ON conjugates with cell lysate from MCF-7, SK-BR-3, BT-20, and MDA-MB-231 breast cancer cells and take relaxation measurements before and after UV-exposure. Single NP-ONs will be used as a negative control (i.e. NP-ONs with only a single c-myc binding domain) (Months 30 - 33).

These studies have not yet commenced.

b. Perform qRT-PCR of c-myc RNA isolated from each breast cancer cell line (Months 30 – 33)

These studies have not yet commenced.

c. Deliver pNP-ON into each breast cancer cell line and take relaxation measurements before and after UV exposure. Single pNP-ONs will be used as a negative control (Months 33 – 36).

These studies have not yet commenced.

KEY RESEARCH ACCOMPLISHMENTS:

- Synthesized dextran-coated iron oxide NPs with hydrodynamic diameters ranging from ~20 nm to ~120 nm
- Synthesized aminated and carboxylated NPs
- Synthesized NPs with R2 relaxation times as high as 381 $mM^{-1}s^{-1}$
- Synthesized relatively monodisperse iron oxide NPs via thermal decomposition.
- Prepared gold-coated iron oxide NPs.
- Using 33 nm NP-ONs we detected as little as 10 pmoles of target
- NP-ON hybridization to complementary DNA targets produced as much as a 41% change in T2 signal.
- Aminated NPs up to 200 nm in diameter were efficiently internalized into cells.
- Internalization of aminated NPs reached saturating levels within just 1 hour when NP concentrations in the media were ~50 ug/mL.

REPORTABLE OUTCOMES

Manuscripts:

Thorek, D.L.J., **Tsourkas, A.** (2008) Size, charge, and concentration dependent uptake of iron oxide nanoparticles by non-phagocytic cells: a comparative study of USPIO, SSPIO, and MPIO. *Biomaterials*. Accepted.

Podium Presentations:

Tsourkas, A. (2008) Magnetic nanoparticle-based detection of RNA transcripts. Department of Defense, Breast Cancer Research Program, Era of Hope Meeting, Baltimore, MD.

Tsourkas, A. (2008) *Molecular imaging: from drug development to the early detection of disease*. Department of Biomedical Engineering 10th Anniversary Symposium, Georgia Institute of Technology, Atlanta, GA.

Tsourkas, A. (2007) *Delineating molecular signatures of disease with novel molecular imaging probes*. Department of Biomedical Engineering Seminar Series, Rutgers University, Piscataway, NJ.

Poster Presentations:

Thorek, L.J., Kimmel, J., Solomon, D., Hoang, D., Lee, H., **Tsourkas, A.** (2008) Magnetic nanoparticle-based detection of RNA transcripts. Department of Defense, Breast Cancer Research Program, Era of Hope Meeting, Baltimore, MD.

Thorek, D., **Tsourkas, A.** (2007) *Magnetic relaxation switch detection of cellular mRNA*. Biomedical Engineering Society, Los Angeles, CA.

Undergraduates Supported by this Award:
Joseph Kimmel, B.S. in Bioengineering, 2008. Will attend Mt. Sinai Medical School in the fall of 2008.

CONCLUSION:
In summary, we have shown that we can synthesize dextran-coated superparamagnetic iron oxide nanoparticles with hydrodynamic diameters ranging from 20 nm to 120 nm. Dynamic light scattering, however, showed that the NPs were not monodisperse and therefore we have also begun making NPs via thermal decomposition. TEM analysis of NPs prepared by thermal decomposition demonstrated a relatively monodisperse population of NPs with an iron oxide core size of ~5 nm. We believe that this alternative NP synthesis method will allow us to more accurately determine the effect of NP size on our ability to detect RNA with NP-ON conjugates since the NPs will have more discrete sizes. Further, this synthetic approach has allowed us to prepare gold-coated iron oxide nanoparticles, which should facilitate ON conjugations.

In parallel to our work with NP synthesis and RNA detection, we have also begun studies to optimize delivery of NPs into cells. In particular, we found that NPs < 200 nm are taken up more efficiently than larger NPs. Therefore, we will focus on NPs within this size range when testing our RNA detection scheme in live cells.

REFERENCES:
1) Thorek, D.L.J., **Tsourkas, A.** (2008) Size, charge, and concentration dependent uptake of iron oxide nanoparticles by non-phagocytic cells: a comparative study of USPIO, SSPIO, and MPIO. *Biomaterials*. Accepted.

2) Park, J., An, K., Hwang, Y., Park, J., Noh, H., Kim, J., Park, J., Hwang, N., Hyeon, T. (2004) Ultra-large-scale syntheses of monodisperse nanocrystals. Nature Materials, 3, 891-895.

Biomaterials xxx (2008) 1–8

Contents lists available at ScienceDirect

Biomaterials

journal homepage: www.elsevier.com/locate/biomaterials

Size, charge and concentration dependent uptake of iron oxide particles by non-phagocytic cells

Daniel L.J. Thorek, Andrew Tsourkas*

Department of Bioengineering, University of Pennsylvania, 210 South 33rd Street, 240 Skirkanich Hall, Philadelphia, PA 19104, USA

ARTICLE INFO

Article history:
Received 25 March 2008
Accepted 16 May 2008
Available online xxx

Keywords:
Molecular imaging
MRI
Ultrasmall superparamagnetic iron oxide
Standard superparamagnetic iron oxide
Micron-sized paramagnetic iron oxide
Nanoparticles

ABSTRACT

A promising new direction for contrast-enhanced magnetic resonance (MR) imaging involves tracking the migration and biodistribution of superparamagnetic iron oxide (SPIO)-labeled cells in vivo. Despite the large number of cell labeling studies that have been performed with SPIO particles of differing size and surface charge, it remains unclear which SPIO configuration provides optimal contrast in non-phagocytic cells. This is largely because contradictory findings have stemmed from the variability and imprecise control over surface charge, the general need and complexity of transfection and/or targeting agents, and the limited number of particle configurations examined in any given study. In the present study, we systematically evaluated the cellular uptake of SPIO in non-phagocytic T cells over a continuum of particle sizes ranging from 33 nm to nearly 1.5 μm, with precisely controlled surface properties, and without the need for transfection agents. SPIO labeling of T cells was analyzed by flow cytometry and contrast enhancement was determined by relaxometry. SPIO uptake was dose-dependent and exhibited sigmoidal charge dependence, which was shown to saturate at different levels of functionalization. Efficient labeling of cells was observed for particles up to 300 nm, however, micron-sized particle uptake was limited. Our results show that an unconventional highly cationic particle configuration at 107 nm maximized MR contrast of T cells, outperforming the widely utilized USPIO (<50 nm).

1. Introduction

Continuing advancements in cell-based therapies have recently led to the emergence of cellular imaging as a strategy to track the migration and biodistribution of target cells in living organisms. Pre-clinical studies have already shown that cellular imaging can be used to evaluate stem cell distribution and homing in cell-based regenerative therapies [1,2]. Recently, cellular imaging has also allowed for improved assessment of functional efficacy and applicability of immunotherapeutic treatments in disease models for cancer [3–5] and AIDS [6].

In addition to evaluating cell-based therapies, cellular imaging also promises to provide a great deal of insight into diverse physio- and pathological phenomena. Interesting applications include the observation of monocyte recruitment to atherosclerotic lesions for the mapping of disease development and therapeutic intervention [7], imaging embryonic stem cell movement during embryonic [8] and organ development [9] and monitoring the dynamics of metastatic cellular extravasation and tissue invasion [10,11].

Tracking of labeled cells has been accomplished with a variety of imaging modalities including optical methods, positron emission tomography (PET), single photon emission computed tomography (SPECT), and magnetic resonance (MR) imaging [12–14]. MR imaging presents a particularly promising approach because of its high spatial resolution in three dimensions and exquisite soft tissue contrast, which can be acquired concomitantly with the contrast-enhanced cellular distribution. MR detection of cells in vivo is often accomplished following labeling with superparamagnetic iron oxide (SPIO) particles. SPIO are negative contrast agents that are typically composed of an iron oxide crystal core surrounded by a polymer or polysaccharide shell [15]. A variety of manifestations of SPIO have been used to track cells, which can be broadly categorized as (1) ultrasmall SPIO (USPIO) with an overall diameter of 30–50 nm [16], (2) standard SPIO (SSPIO) with a diameter of 50–150 nm and (3) micron-sized paramagnetic iron oxide (MPIO) having a diameter approaching or greater than 1 μm [17].

To date, USPIO has perhaps been the most widely utilized SPIO configuration for cell labeling. Although they provide less contrast enhancement per particle compared with SSPIO and MPIO, large numbers of particles can be loaded into each cell [18,19]. As cationic surfaces have been shown to facilitate cellular internalization [20,21], USPIO is often modified with polycationic cell permeating peptides (CPPs) such as HIV transactivator (TAT) [22] or protamine [23]. Other transfection techniques, sometimes in concert with CPPs, are also used [24,25].

* Corresponding author. Tel.: +1 (215)898 8167; fax: +1 (215)573 2071.
E-mail address: atsourk@seas.upenn.edu (Andrew Tsourkas).

0142-9612/$ – see front matter © 2008 Elsevier Ltd. All rights reserved.
doi:10.1016/j.biomaterials.2008.05.015

An exciting new direction for cell tracking involves labeling cells with MPIO [26]. The large iron oxide cores present in these particles provide enough contrast for single cells to be imaged by MR. However, work with such large particles generally confines application of iron oxide labeling to phenotypes such as macrophages [18], dendritic cells [27] or hepatocytes that actively internalize foreign material. MPIO uptake in non-phagocytic cells has been accomplished, but is limited by the additional conjugation work and cost of using an antibody-mediated approach [28], which must be species specific and may induce adverse cellular events.

Recently, several studies have attempted to define an optimized particle configuration for iron oxide labeling of both phagocytic and non-phagocytic cell types. Although MPIO was excluded from all of these studies, it was found that phagocytic monocytes are more effectively labeled with SSPIO (150 nm) compared with USPIO (30 nm) [18,29]. Further, it was found that ionic carboxydextran-coated SSPIO (i.e. ferucarbotran) performed better than non-ionic dextran-coated SSPIO (i.e. ferumoxide) [18]. It remains unclear how MPIO compares with these agents; however, single cell detection has been achieved in phagocytic cells with both SPIO configurations [30,31].

The optimal SPIO configuration for labeling non-phagocytic cells has been much more elusive and findings have been contradictory. For example, in one study it was found that the delivery of carboxydextran USPIO and dextran-labeled SSPIO into non-phagocytic cancer cells and leukocytes (with the assistance of lipofection agents) was similar in terms of iron uptake [21]. Both particles led to higher iron uptake than USPIO. This indirectly suggests that larger particles with ionic coatings are superior to non-ionic USPIO. However, in a different study it was found that, in the presence of poly-L-lysine, ionic (aminated) USPIO exhibited significantly higher iron uptake in non-phagocytic cells compared with SSPIO. These data suggest that smaller ionic particles are internalized into non-phagocytic cells more efficiently [32]. These contradictory findings likely stem from the variability and imprecise control over surface charge and the limited number of particle configurations examined, particularly with respect to diameter (ranging only from ~17 nm to 150 nm).

In the present study we systematically evaluated the cellular uptake of SPIO in non-phagocytic T cells over a continuum of particle sizes ranging from 33 nm to nearly 1.5 μm and with precisely controlled surface properties. T cells were selected as a model non-phagocytic phenotype since visualization of their distribution is expected to be of importance for adoptive T cell therapy for cancer and T cell homing in autoimmune diseases. Extremely fine control was exerted on the surface properties of SPIO by direct chemical modification of particle surfaces rather than attempting to modulate the density of supplemental transfection agents. Concentration effects and incubation times were also tested in the interest of isolating the role particle size exerts on individual cell uptake and overall contrast enhancement. Our work shows that in a space between USPIO and MPIO exist configurations of relatively small particles (~100 nm) that efficiently label non-adherent, non-phagocytic T cells and generate higher relaxivity (per cell) relative to particles of other sizes.

2. Materials and methods

2.1. Nanoparticle synthesis

Three different formulations of dextran-coated superparamagnetic iron oxide nanoparticles were prepared using the co-precipitation method [33]. All three formulations were prepared following the same procedure, as described below, with the only difference being the amount of $FeCl_2$ and $FeCl_3$ added. Specifically, 25 g of dextran T10 (GE Healthcare, Piscataway, NJ) was dissolved in 50 mL of dH_2O and heated to 80 °C for 1 h. The solution was allowed to return to room temperature and continued to mix overnight. Subsequently, the dextran was cooled to 4 °C on ice and degassed with N_2 for 1 h. $FeCl_2$ (0.7313 g, 1.5 g, or 2.2 g) and $FeCl_3$ (1.97 g, 4 g, or 6 g, respectively) were each rapidly dissolved in 12.5 mL of degassed dH_2O and kept on ice for approximately 10 min. The iron solutions were added to the dextran simultaneously and allowed to mix for 30 min. Keeping this mixing solution at 4 °C, 15 mL of ammonium hydroxide was added. The resulting black viscous solution was then heated to 90 °C for 1 h then cooled overnight, followed by ultracentrifugation at 20 k rcf for 30 min. Pellets were discarded and the supernatant was continually diafiltrated using a 100-kDa MWCO cartridge (GE Healthcare) on a peristaltic pump (E323, Watson Marlow Bredel, Wilmington, MA). The particles were exchanged into 0.02 M citrate, 0.15 M sodium chloride buffer until all unreacted products had been removed. Aminated silica-coated iron oxide micro-particles were purchased from Bioclone Inc. (San Diego, CA). Amine functionalized styrene copolymer-coated iron oxide particles (Adembeads) were purchased from Ademtech SA (Pessac, France).

2.2. Amination of particles

Amination and crosslinking of the coating on the dextran–SPIO were accomplished through reaction of the SPIO with 25% 10 M NaOH and 33% epichlorohydrin [34]. After mixing for 24 h, additional ammonium hydroxide was added to the solution, bringing the volume fraction to 25% ammonium hydroxide, and the reaction was allowed to proceed for another 24 h. The particles were then exhaustively purified via diafiltration. The resulting particles were amine functionalized crosslinked iron oxide.

2.3. FITC labeling and amine-blocking of particles

All SPIO particles were labeled with FITC at a FITC-to-iron molar ratio of 19.2:1. FITC was reacted with particles for 4 h followed by two rounds of gel purification, once on a NAP-5 column and then on a PD10 column (GE Healthcare), both equilibrated with PBS. The FITC-labeled SPIO was subsequently reacted with various volumes of glycidol (0.01–50%) to produce populations of particles with different amine content. The particles were cleaned of excess glycidol through repeated precipitation in isopropanol and resuspension in PBS. Amine-blocking was also attempted with particles of 200 nm and greater, but this modification impelled immediate particle insolubility.

2.4. Measurement of particle size

The hydrodynamic diameter of the dextran-coated and commercial iron oxide particles was measured using a Zetasizer Nano-z (Malvern Instruments, Malvern, UK) through dynamic light scattering (DLS). The dextran-coated SPIO particles were diluted in PBS to a concentration of approximately 0.5 mg/mL and read in triplicate. The commercial particle diameters were read in the same manner, but only after undergoing three washes by precipitation in the presence of a strong magnet and resuspension in PBS. The values reported for all samples are the intensity peak values.

2.5. Measurement of particle cores

Transmission electron micrographs of all iron oxide particles were taken using a JEOL 2010 at 200 kV. Samples were prepared for imaging by evaporating the particles onto a carbon-coated copper grid (Holey carbon – mesh 200, Structure Probe Inc., West Chester, PA). Salt was removed from all of the samples prior to evaporation by exchanging the particles into dH_2O. Images of particle cores were analyzed using ImageJ (National Institutes of Health, Bethesda, MD). Since many of the particles were found to be composed of a cluster of multiple iron oxide cores, the average diameter of each core and the average number of cores per particle were determined. Assuming each core to be spherical, the amount of iron per particle type was determined from the aggregate core volume.

2.6. Measurement of particle relaxivity (R_1 and R_2)

The longitudinal (R_1) and transverse (R_2) relaxivity of each particle was calculated as the slope of the curves $1/T_1$ and $1/T_2$ against iron concentration, respectively. T_1 and T_2 relaxation times were determined using a Bruker mq60 MR relaxometer operating at 1.41 T (60 MHz). T_1 measurements were performed by collecting 12 data points from 5.0 ms to 1000 ms with a total measurement duration of 1.49 min. T_2 measurements were made using $\tau = 1.5$ ms and two dummy echoes, and fitted assuming monoexponential decay.

2.7. Measurement of number of amines per particle

The number of amines per particle was determined following the general procedure described by Zhao et al. [35]. Briefly, iron oxide particles at a concentration of 2 mg/mL Fe were reacted with excess *N*-succinimidyl 3-(2-pyridyldithio) propionate (SPDP, Calbiochem, San Diego, CA) for 4 h. SPIO was washed of excess SPDP through repeated precipitation in isopropanol and resuspension in PBS. The particles were then run through a 50-kDa MWCO centrifugal filter (YM-50, Millipore, Billerica, MA) either with or without the addition of disulfide cleavage agent TCEP. The difference of the absorbance of these two samples at 343 nm was used to determine the

Please cite this article in press as: Daniel L.J. Thorek, Andrew Tsourkas, Size, charge and concentration dependent uptake of iron oxide particles by non-phagocytic cells, Biomaterials (2008), doi:10.1016/j.biomaterials.2008.05.015

concentration of SPDP in the filter flow. Adjusting for dilution, the number of amines per particle was determined.

2.8. Cell culture and labeling

Immortalized human T cells, Jurkat Clone E6-1 (ATCC), were maintained at 37 °C in 5% CO_2 in RPMI 1640 (Mediatech, Manassas, VA) media supplemented with 10% FBS (Hyclone, Logan, UT) and penicillin/streptomycin (Mediatech). T cells were labeled with iron oxide particles by incubating the commercial and lab-made particles with 2×10^6 cells in 400 μL of fully supplemented media for 1 h or 4 h, at 37 °C in 5% CO_2. Cells were washed of non-internalized particles through two methods. Synthesized dextran-coated particles were washed from cells using centrifugation. Specifically, cells were pelleted at 0.5 rcf for 5 min and resuspended in PBS. This was repeated three times. The dextran-coated particles are highly soluble in aqueous solvents and do not precipitate at these centrifugation speeds. Removal of non-internalized commercial particles was accomplished through a density gradient. The cells and particles were diluted to 1 mL with PBS and overlayed on 4 mL of room temperature Ficoll-Paque PLUS (GE Healthcare). The sample was centrifuged at 0.4 rcf for 40 min. Cells loaded with particles were retrieved from the interface layer. To determine if particles were internalized or merely adsorbed on the cell exterior, surface receptor cleavage enzyme trypsin was used. Following particle incubation, as described above, cells were exposed to 0.025% trypsin–EDTA (Invitrogen) for 5 min. Purification of non-internalized particles was carried out as detailed. No statistical difference was seen in either flow cytometry or relaxometry between groups washed with or without enzyme.

2.9. Flow cytometry and relaxation measurements

Immediately after non-internalized iron oxide particles were removed from T cell samples, flow cytometry was performed on a Guava Easycyte (Guava Technologies, Hayward, CA). For labeling and viability experiments, forward and side scatterings were used to identify the entire population of cells. Data analysis of flow cytometry data was accomplished with FlowJo (TreeStar, Ashland, OR). Viability of T cells was determined using the LIVE/DEAD cytotoxicity kit for mammalian cells (Invitrogen, Carlsbad, CA) according to the manufacturer's instructions. In order to evaluate the decrease in T_2 relaxation time of iron oxide internalized T cells, purified cells were lysed for 30 min in 0.1% SDS in PBS at 37 °C. Samples were diluted to 0.5×10^6 cells/mL in 300 uL and T_2 relaxation times were measured using the benchtop relaxometer. All flow and magnetic resonance measurements were made in triplicate on at least two separate occasions.

3. Results and discussion

3.1. Particle synthesis and characterization

Three different formulations of dextran-coated superparamagnetic iron oxide nanoparticles were prepared via co-precipitation. All three syntheses utilized a ratio of approximately three ferrous to ferric iron chloride; however, the total amount of iron was increased by whole numbers, i.e. 2× and 3× irons, respectively. This deviation in the amount of iron present during synthesis allowed for the manufacture of SPIO with a range of different sizes and properties. Specifically, DLS of the SPIO, following crosslinking and amination of the dextran coating, indicated average hydrodynamic radii of 33.4 nm, 53.5 nm and 107 nm, respectively, with the larger nanoparticles corresponding to syntheses that utilized more iron. When the total amount of iron was increased further, the co-precipitation solution became extremely viscous and yielded highly dispersed aggregates that precipitated out of solution. Therefore, nanoparticles ranging from 200 nm to 1 μm in diameter were acquired from commercial sources. Specifically, superparamagnetic iron oxide particles of 200 nm and 300 nm diameter with an amine functionalized styrene copolymer coating (Amino–Adembeads) were purchased from Ademtech, while amine functionalized silica-coated 1 μm diameter particles were purchased from Bioclone. This allowed particle sizes across nearly three orders of magnitude to be compared.

The particle sizes as determined by DLS, peak intensity values, are compared in Fig. 1. The 33.4 nm, 53.5 nm and 107 nm dextran-coated SPIO samples were fully soluble at physiological conditions. Conversely, it was found that the large size of the 289 nm and 1430 nm particles led to rapid precipitation. Settling was also a concern for the 207 nm particles; however, full precipitation generally took several hours.

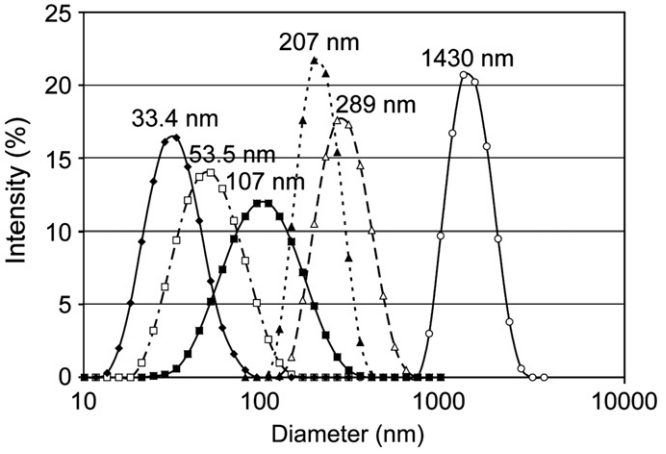

Fig. 1. Hydrodynamic diameter of SPIO. The hydrodynamic diameter of SPIO particles was determined by DLS. Intensity measurements are reported and the peak intensity is provided for each distribution.

Analysis of the iron oxide core size and structure of the magnetic particles was conducted using TEM. Representative micrographs are shown in Fig. 2. Aggregation of particles in salt free solution was a problem during TEM sample preparation; however, reduction in sample concentration allowed for imaging of discretely distributed particles. Iron cores were easily distinguished from carbon-coated copper grids, while dextran and styrene copolymer were not visible because of their low electron density.

An interesting feature of the dextran-coated nanoparticles is that each particle consists of a cluster of one or more iron oxide cores, with each core being approximately equal in size. Specifically, the distribution of cores is centered at approximately 6 nm for all three dextran-coated nanoparticles (Fig. 3); however, the average number of cores per particle increases with overall hydrodynamic diameter. In contrast, the larger 207 nm and 289 nm styrene copolymer-coated particles exhibited a single large spherical iron oxide core, while the 1.43 μm silica-coated particles exhibited an amorphous iron oxide core of no discrete size or shape. A summary of the properties of each SPIO is provided in Table 1.

The R_1 and R_2 data (Figs. 4 and 5), also summarized in Table 1, indicate that there is a trend of increasing R_2 and decreasing R_1 with size up to the 107 nm particles. For particles of greater size, the single large core of the 207 nm and 289 nm particles does not translate into proportionately higher R_2. This likely reflects lower crystallinity of the larger single iron oxide cores in comparison to smaller crystals [36]. Furthermore, according to the Solomon–Bloembergen theory, which relates the relaxation rate to particle properties, the total size of the particle is not critical to the magnitude of R_2 as the susceptibility effect falls off from the surface with an exponential (r^6) dependence [37,38]. It should be noted that the R_1 values reported for particles greater than 200 nm are likely underestimates due to precipitation of the particles during T_1 measurements. For instance, determining T_1 relaxation times required more than 100 s per sample, which was an ample time for the micrometer-sized particles to precipitate out of solution.

3.2. Cell loading

The extent to which T cells internalize iron oxide particles is not only dependent on particle size but also various other particle characteristics and cell loading conditions, including surface charge, particle concentration, and incubation time. Thus, before it

Please cite this article in press as: Daniel L.J. Thorek, Andrew Tsourkas, Size, charge and concentration dependent uptake of iron oxide particles by non-phagocytic cells, Biomaterials (2008), doi:10.1016/j.biomaterials.2008.05.015

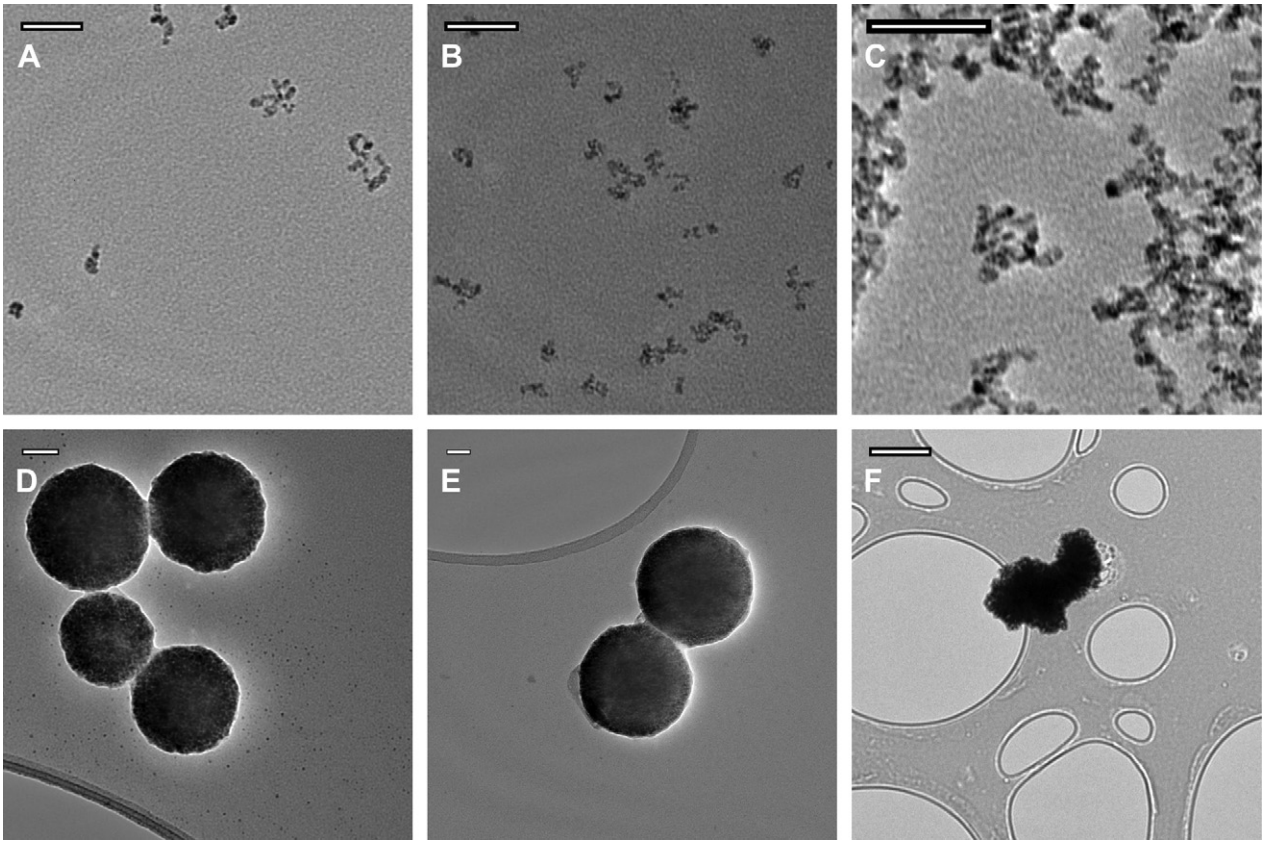

Fig. 2. TEM of SPIO cores. High magnification transmission electron microscopy images of the iron oxide particles were obtained with a JEOL 2010 operating at 200 kV. Structure analysis revealed the multiple core nature of the (A) 33.4 nm, (B) 53.5 nm and (C) 107 nm dextran-coated SPIO. Larger particles were composed of single cores; (D) 207 nm, (E) 289 nm and (F) 1430 nm. All scale bars are 50 nm, excluding (F) 1 μm.

could be determined which particle size led to the highest relaxivity per cell, it was first necessary to identify conditions whereby cell loading was independent of these other parameters. The use of fluorescently labeled iron oxide particles combined with flow cytometry provided a facile method by which particle uptake could be systematically assessed in a high-throughput manner. In the current study, all SPIO samples were fluorescently labeled with an equivalent amount of FITC/iron.

3.2.1. Concentration

In order to confirm that iron oxide particles were present in sufficient quantity for maximum cellular uptake, T cells were incubated with increasing iron concentrations until a saturating level was reached. As shown in Fig. 6, dextran-coated particles were efficiently internalized, all reaching a plateau at iron concentrations below 50 μg/mL. Greater than 100 μg/mL was required to saturate the loading of the 207 nm, 289 nm and 1430 nm particles. The necessity for these higher iron concentrations may be attributed to the fact that the number of particles per unit of iron is far less than the smaller agents. Further, there is likely less contact between the larger particles and the suspended cells because of their continual sedimentation. This was perhaps most evident with MPIO, where cell labeling was poor across all particle concentrations. Even at 1000 μg/mL (data not shown) labeling with MPIO did not reach the levels achieved by the dextran-coated USPIO and SPIO.

3.2.2. Surface properties

Surface charge is important for intracellular delivery of exogenous material. This principle has been described for a variety of nanoparticle (examples include gold [39], polymer [40,41] and silica [42]) and biological (for example, delivery of DNA with cationic proteins, lipids and polymers [43]) contexts. The aminated surfaces of the particles used in this study provide an inherent surface charge, facilitating cellular interaction. However, in order to study the role this property has in the intracellular delivery of iron oxide contrast agent, it is necessary to manipulate the magnitude of the surface charge. To do so we have applied glycidol, a hydroxyl terminating epoxide, to generate subsets of particles with a gradient of surface amines. Glycidol has been used previously in dendrimer chemistry to reduce the chemotoxicity of highly-positively charged dendrimers [44]. The tight control of surface properties produced by consuming amines with glycidol allows for isolated examination and evaluation of the role of surface charge on SPIO.

The summary of particle uptake on a per cell basis is shown in Fig. 7(A–C). Each data point represents the normalized mean fluorescence intensity (MFI) of T cells that were incubated with iron oxide particles at a saturating concentration (previously determined) for 4 h. Under these incubation conditions, it was found that particles in their natural (fully aminated) state are maximally internalized. Any further increase in the positive surface charge will not further augment SPIO loading. In other words, the efficiency of cell labeling has become independent of surface charge. In all cases, uptake and internalization of the particles were rapid. Representative uptake of the 107 nm particles as a function of time is shown in Fig. 7(D).

3.2.3. Viability

The impact and potential cytotoxicity of each iron oxide particle on T cells were measured using a two-color fluorescent cell viability kit. Negligible to low levels of cell death were observed (Fig. 8) for all particles at diminished and saturating concentrations of iron oxide (10 μg/mL and 50 μg/mL, respectively). The exception was for

Please cite this article in press as: Daniel L.J. Thorek, Andrew Tsourkas, Size, charge and concentration dependent uptake of iron oxide particles by non-phagocytic cells, Biomaterials (2008), doi:10.1016/j.biomaterials.2008.05.015

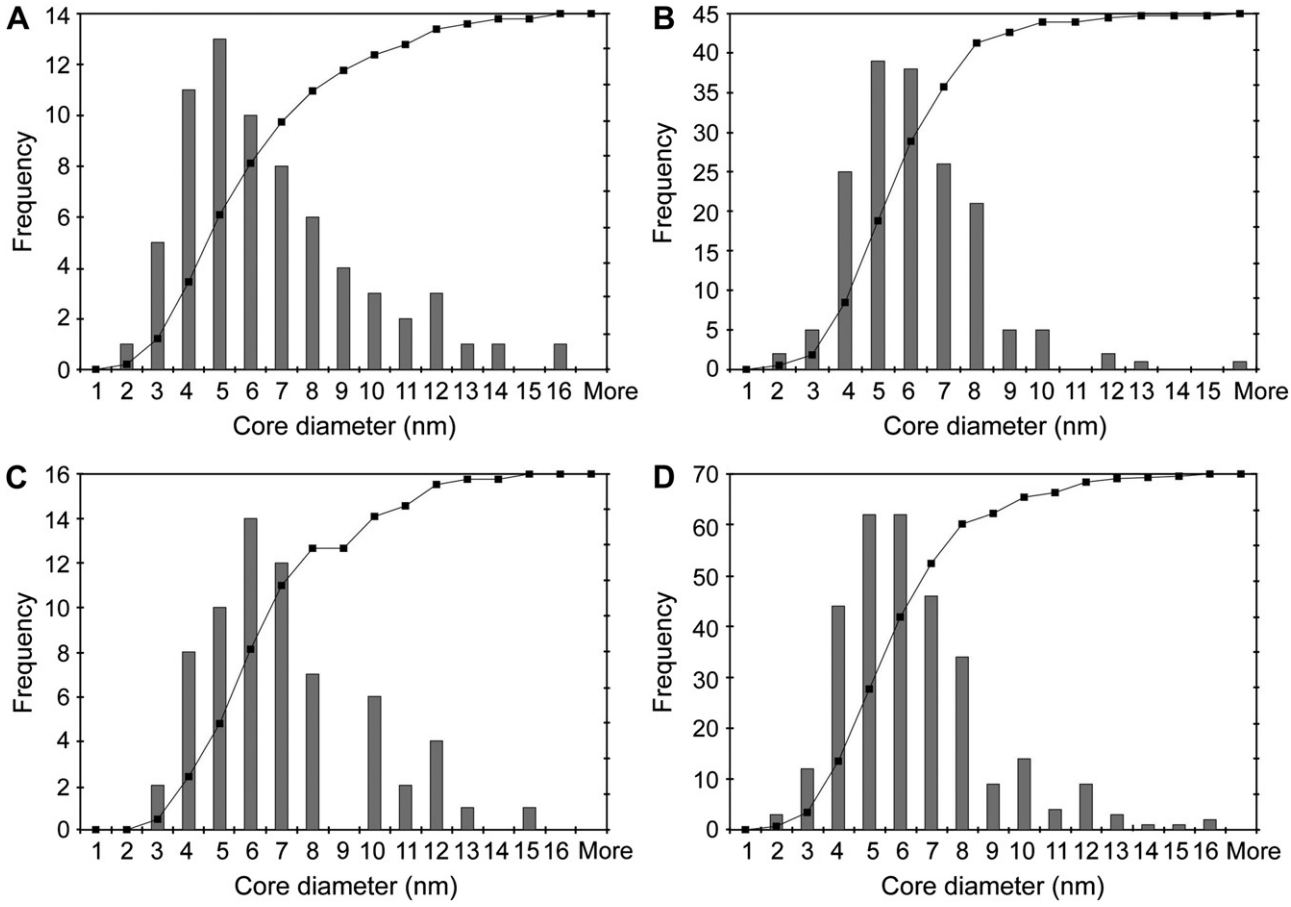

Fig. 3. Size distribution of SPIO core diameters. TEM measurements of the SPIO core diameter for (A) 33.4 nm, (B) 53.5 nm, (C) 107 nm and (D) all cores. The cores diameters were analyzed assuming that they were spherical and the frequency and cumulative distributions are plotted. Particle size appears to be determined by the number of cores per particle rather than the size of those constituent cores.

Table 1
Physical and magnetic properties of SPIO

Hydrodynamic diameter (nm)	Core diameter (nm)	Number of cores	R_2 (/mM/s)	R_1 (/mM/s)[a]	R_2/R_1	NH_2/particle	Fe (atoms)/particle[b]	Coating material
33	6.067	1.9	71.00	13.56	5.24	185	8924	Dextran
53	5.603	5.3	82.25	9.97	8.25	631	20,065	Dextran
107	6.534	11.2	381.00	7.24	52.66	1024	66,729	Dextran
207	175.4	1	176.58	0.51	344.48	6.0×10^5	6.3×10^7	Styrene copolymer
289	289.6	1	115.20	0.34	337.43	2.2×10^6	2.6×10^8	Styrene copolymer
1430	–	1	64.32	0.41	156.49	8.5×10^8	1.3×10^7	Silica

[a] R_1 values for 207 nm, 289 nm and 1430 nm particles may be underestimated due to precipitation during measurements.
[b] Measurement of Fe (atoms)/particle for the commercial particles was made using the company provided relative iron mass per particle data, rather than the core size determination from TEM.

the 107 nm SPIO, which exhibited some adverse cell influence even at 10 μg/mL. This effect was exacerbated at increased concentrations. When the amines on the 107 nm particle were completely blocked, cell death was reduced to negligible levels; however, internalization was also reduced to negligible levels (Fig. 7C). T cell death is likely attributable to the high positive surface charge possessed by the SPIO. Similar results have been seen with amine-terminated poly(amidoamine) dendrimers [45]. The extremely high driving force for cell internalization imparted by positive SPIO surface charge can lead to cell death.

In order to minimize the toxicity of the 107 nm particles, the incubation time with T cells was decreased to 1 h. As shown in Fig. 7D, particle uptake is still saturated within this time frame, therefore exposing T cells to excess SPIO for longer periods of time was deemed unnecessary. No toxicity was observed with the 107 nm particles after just 1 h of incubation.

3.2.4. Magnetic contrast enhancement

Flow cytometry was utilized to determine the saturating conditions for each SPIO; however, these single cell measurements were conducted with some variation between the number of fluorescent labels per particle making it difficult to accurately quantify the number of particles per cell. Also, after labeling cells with superparamagnetic tracking agents the critical assessment of ability to track cells is their relaxivity. Therefore, a benchtop NMR minispectrometer, near the clinical field strength of 1.5 T, was utilized for evaluating in vitro loading. As shown in Fig. 9, T cells loaded with particles showed a dose-dependent, negative contrast enhancement.

As befits their widespread application in the literature, the USPIO proved effective at lowering the spin–spin relaxation time (T_2). Despite delivering only a small payload of iron per particle, the large numbers of 33.4 nm and 53.5 nm particles that accumulate in

Please cite this article in press as: Daniel L.J. Thorek, Andrew Tsourkas, Size, charge and concentration dependent uptake of iron oxide particles by non-phagocytic cells, Biomaterials (2008), doi:10.1016/j.biomaterials.2008.05.015

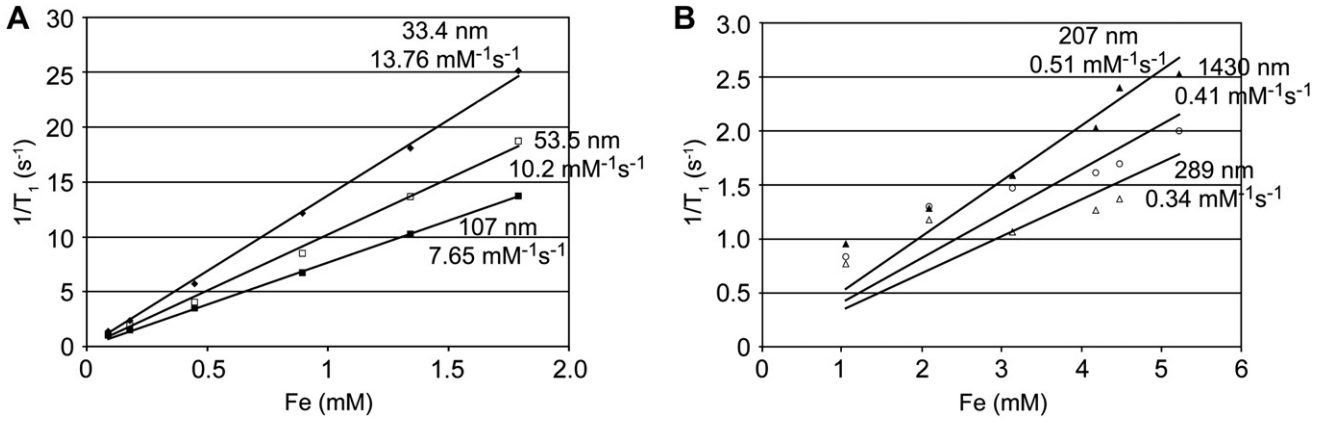

Fig. 4. T_1 relaxivity (R_1) measurements of SPIO. SPIO of various sizes were diluted in PBS to iron concentrations between (A) 0.1 mM and 2 mM or (B) 1 mM and 6 mM. T_1 values were then obtained using the minimum time sequence required to get reproducible values, because of precipitation issues. The inverse of the T_1 time, in seconds, was linearly fit against concentration to yield the particle R_1.

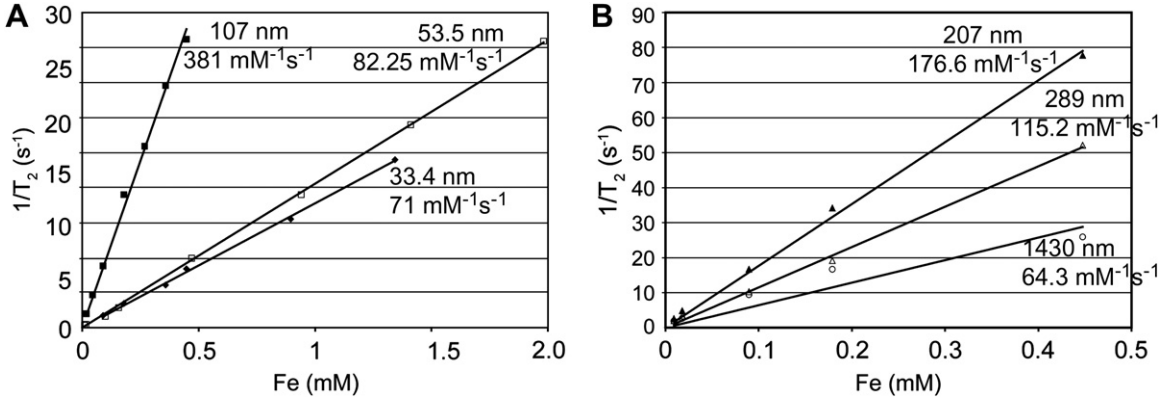

Fig. 5. T_2 relaxivity (R_2) measurements of SPIO. SPIO of various sizes were diluted in PBS to iron concentrations between (A) 0.1 mM and 2 mM or (B) 0.01 mM and 0.5 mM. The T_2 values were then obtained using a monoexponential curve fit. The inverse of these values, plotted against concentration, gives the R_2. Precipitation of the 1430 nm particles resulted in nonlinearity.

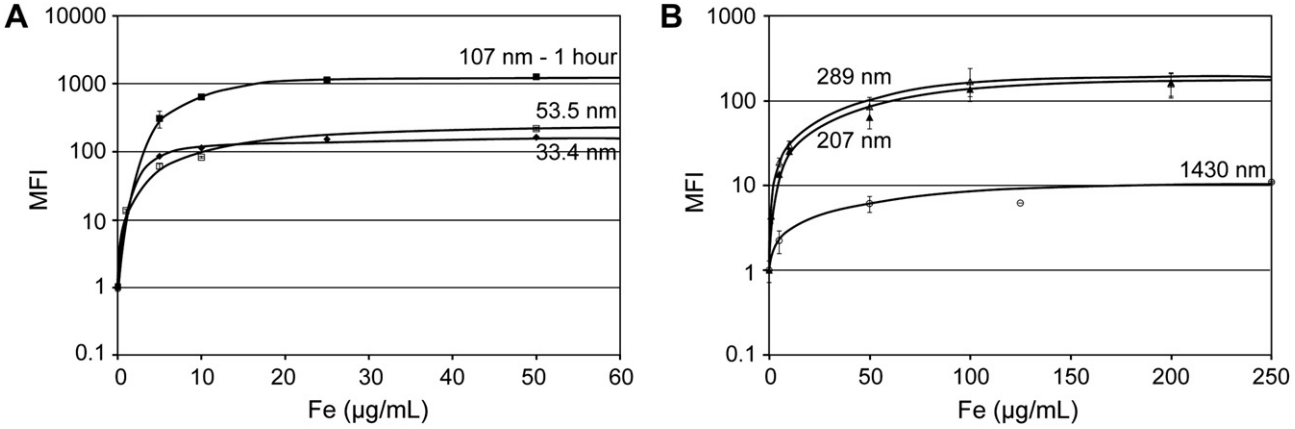

Fig. 6. Dependence of SPIO loading on particle concentration. Fluorescently labeled SPIO of various sizes and across a range of concentrations was incubated with 2×10^6 T cells/mL at 37 °C for 4 h (excluding the 107 nm particle as indicated). SPIO uptake was then measured by flow cytometry. Each experiment was conducted in triplicate on at least two separate occasions and each data point represents the average value for the mean fluorescent intensity (MFI). Note the difference in x- and y-axes for (A) and (B).

the cells allow for a strong aggregate effect, producing an average T_2 signal of 126.05 ms and 51.5 ms under saturating conditions, respectively. These reduced signal values correlate to an 8.04 and 19.68 times reduction in signal from T cells without any contrast agent ($T_2 = 1013$ ms).

Performance of particles greater than 200 nm was ranked inversely with diameter. Greater concentrations of large particles continued to reduce the T_2 signal; however, when the iron concentration was increased above 500 μg/mL the methods used to distinctly separate loaded-cells from free particles became less reliable. It should be noted that this drawback does not exist for the flow cytometry measurements, as the particles themselves could be excluded from the cells based on forward and side scatter. At 150 μg/mL Fe, the spin–spin relaxation signal from the 207 nm,

Please cite this article in press as: Daniel L.J. Thorek, Andrew Tsourkas, Size, charge and concentration dependent uptake of iron oxide particles by non-phagocytic cells, Biomaterials (2008), doi:10.1016/j.biomaterials.2008.05.015

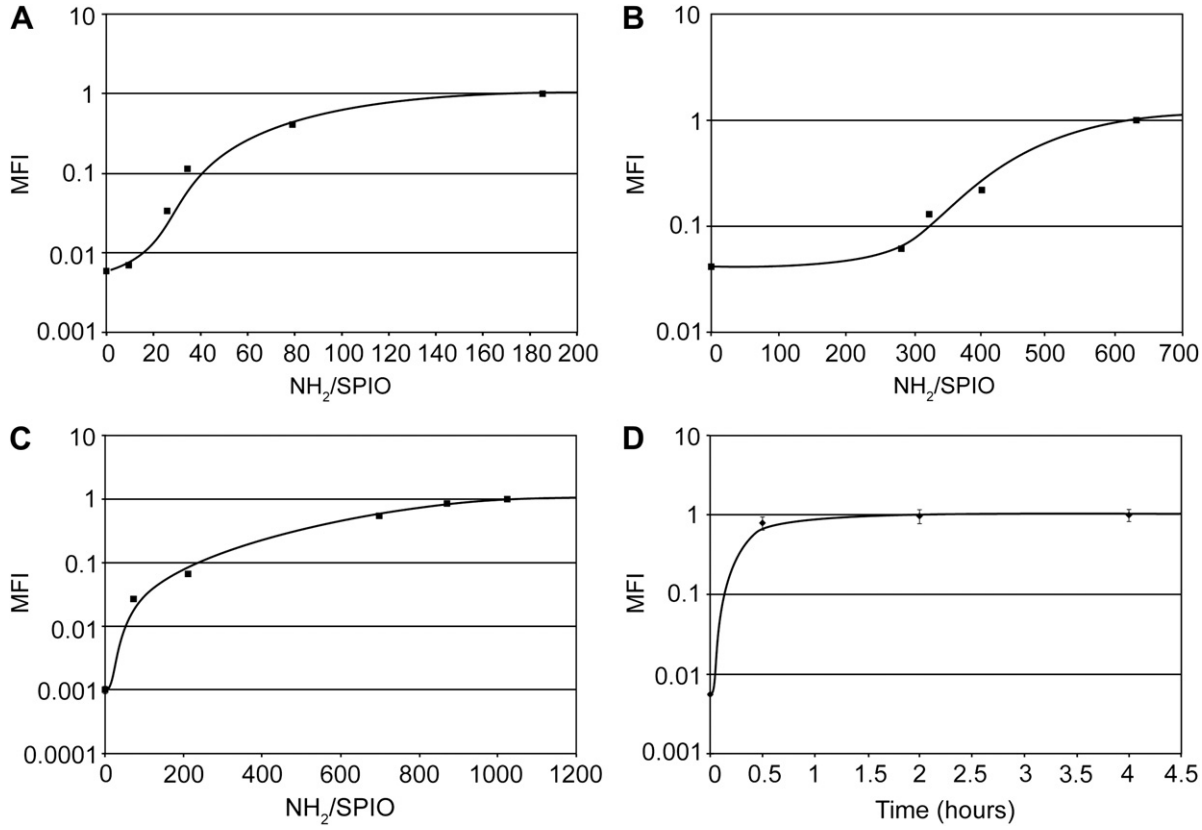

Fig. 7. Dependence of SPIO loading on surface charge. T cell uptake of fluorescently labeled SPIO as a function of surface charge was examined by modulating the number of amines per particle for the (A) 33.4 nm, (B) 53.5 nm and (C) 107 nm particles. A gradient in the degree of functionalization was produced by glycidol blocking of amines. SPIO was incubated with T cells at saturating concentrations, 50 μg/mL, under identical conditions. Flow cytometry was then performed to assess the relative uptake of each SPIO. Each data point represents the mean fluorescent intensity (MFI). The loading of SPIO was rapid; Fig. 7(D) shows the representative uptake of fully-aminated 107 nm particles.

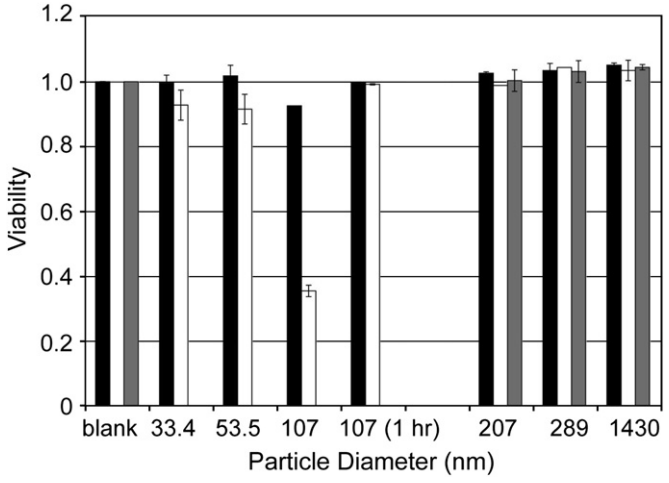

Fig. 8. Viability of T cells incubated with SPIO. SPIO was incubated with T cells at various iron concentrations: 10 μg/mL [black], 50 μg/mL [white] and 100 μg/mL [grey]. After 4 h (unless otherwise noted), viability was measured and normalized to cells grown in the absence of any particles (blank). All SPIO exhibited negligible impact on cell survival after 4 h, excluding the 107 nm diameter particles. Reducing incubation time of these particles to 1 h eliminated adverse effects at both low and saturating concentrations.

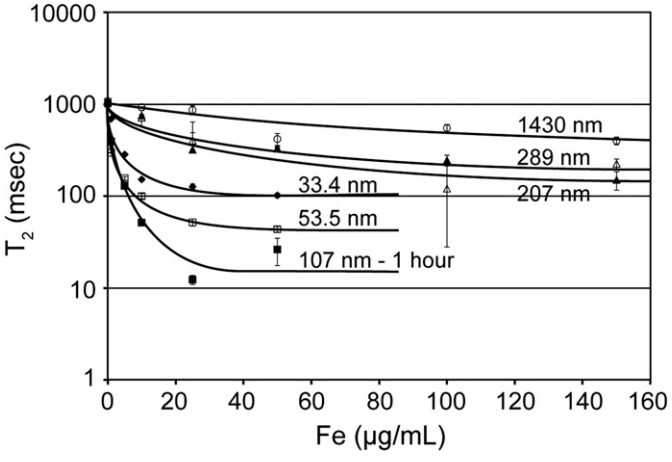

Fig. 9. T_2 relaxation times of T cells labeled with SPIO. T cells were labeled with SPIO of various sizes and across a range of concentrations. The T_2 relaxivity of 0.5×10^6 SPIO-loaded T cells/mL in 300 μL was measured on a Bruker mq60 MR relaxometer operating at 1.41 T (60 MHz). The signal decrease observed following internalization of SPIO is dose-dependent and saturation correlates well with values determined by flow cytometry. The 107 nm SSPIO produced maximum signal decrease.

289 nm and 1430 nm particles was 149.75 ms, 224.3 ms and 398 ms. These findings suggest that despite their high R_2 values and large iron content, particles greater than 200 nm seem to have limited applicability in labeling non-phagocytic cells.

The highly-aminated SPIO with a diameter of 107 nm produced the greatest contrast enhancement. These particles combined the high degree of internalization of the USPIO with the superior relaxivity of larger particles. At the 1 h loading time, to avoid any longer term cytotoxic events, these SSPIO were able to reduce signal approximately two orders of magnitude, providing T_2 signal of only 12.25 ms, or an 82.74 times reduction in signal from control. This reduction in signal was approximately five and 10 times greater than that produced by the 53.5 nm and 33.4 nm SPIO (for the same concentration).

Please cite this article in press as: Daniel L.J. Thorek, Andrew Tsourkas, Size, charge and concentration dependent uptake of iron oxide particles by non-phagocytic cells, Biomaterials (2008), doi:10.1016/j.biomaterials.2008.05.015

4. Conclusions

In this work, efficient iron oxide labeling, without the use of cell penetrating peptides or transfection agents, was accomplished in a clinically relevant non-phagocytic cellular system. The level of SPIO loading in T cells was determined by flow cytometry and verified through evaluation of MR contrast enhancement. Using conditions under which cell loading was independent of particle concentration, chemical surface modification, and incubation time, particle size was isolated as an attribute to affect nano- and microparticle loading. Large particles, over 200 nm in diameter, possess much greater amounts of iron per particle, and thus theoretically require few particles or a single particle per cell in order to be used. However, they suffered from gravitational sedimentation, decreased efficiency of cell labeling, and in some cases free particles were incompletely removed from labeled cells. This may not be a problem with adherent and/or phagocytic cell systems, but significantly hampered their efficacy as magnetic labeling probes for non-phagocytic suspended cells. The vastly greater number of USPIO that accumulate within the cells made up for their weaker R_2 values. While a general trend correlating increased or decreased particle size with labeling was not observed, it was clear that the 107 nm SPIO manifestation led to the largest T_2 signal decrease.

Acknowledgments

D.L.J.T. was supported by NIH T32 HL007954-07, Multidisciplinary Training in Cardiovascular Biology. This work was supported in part by Wyeth Pharmaceuticals, the Transdisciplinary Program in Translational Medicine and Therapeutics, the Lupus Research Institute, and the DOD Breast Cancer Research Program of the Office of the Congressionally Directed Medical Research Programs (BC061856).

References

[1] Bulte JW, Douglas T, Witwer B, Zhang SC, Strable E, Lewis BK, et al. Magnetodendrimers allow endosomal magnetic labeling and in vivo tracking of stem cells. Nat Biotechnol 2001;19(12):1141–7.
[2] Rogers WJ, Meyer CH, Kramer CM. Technology insight: in vivo cell tracking by use of MRI. Nat Clin Pract Cardiovasc Med 2006;3(10):554–62.
[3] Ahrens ET, Flores R, Xu HY, Morel PA. In vivo imaging platform for tracking immunotherapeutic cells. Nat Biotechnol 2005;23(8):983–7.
[4] Pittet MJ, Grimm J, Berger CR, Tamura T, Wojtkiewicz G, Nahrendorf M, et al. In vivo imaging of T cell delivery to tumors after adoptive transfer therapy. Proc Natl Acad Sci U S A 2007;104(30):12457–61.
[5] Sauer MG, Ericson ME, Weigel BJ, Herron MJ, Panoskaltsis-Mortari A, Kren BT, et al. A novel system for simultaneous in vivo tracking and biological assessment of leukemia cells and ex vivo generated leukemia-reactive cytotoxic T cells. Cancer Res 2004;64(11):3914–21.
[6] Sundstrom JB, Mao H, Santoianni R, Villinger F, Little DM, Huynh TT, et al. Magnetic resonance imaging of activated proliferating rhesus macaque T cells labeled with superparamagnetic monocrystalline iron oxide nanoparticles. J Acquir Immune Defic Syndr 2004;35(1):9–21.
[7] Kircher MF, Grimm J, Swirski FK, Libby P, Gerszten RE, Allport JR, et al. Noninvasive in vivo imaging of monocyte trafficking to atherosclerotic lesions. Circulation 2008;117(3):388–95.
[8] Hadjantonakis AK, Papaioannou VE. Dynamic in vivo imaging and cell tracking using a histone fluorescent protein fusion in mice. BMC Biotechnol 2004;4.
[9] Puri S, Hebrok M. Dynamics of embryonic pancreas development using real-time imaging. Dev Biol 2007;306(1):82–93.
[10] Voura EB, Jaiswal JK, Mattoussi H, Simon SM. Tracking metastatic tumor cell extravasation with quantum dot nanocrystals and fluorescence emission-scanning microscopy. Nat Med 2004;10(9):993–8.
[11] Cahill KS, Gaidosh G, Huard J, Silver X, Byrne BJ, Walter GA. Noninvasive monitoring and tracking of muscle stem cell transplants. Transplantation 2004;78(11):1626–33.
[12] Yoneyama R, Chemaly ER, Hajjar RJ. Tracking stem cells in vivo. Ernst Schering Res Found Workshop 2006;60:99–109.
[13] Zhang SJ, Wu JC. Comparison of imaging techniques for tracking cardiac stem cell therapy. J Nucl Med 2007;48(12):1916–9.
[14] Hoshino K, Ly HQ, Frangioni JV, Hajjar RJ. In vivo tracking in cardiac stem cell-based therapy. Prog Cardiovasc Dis 2007;49(6):414–20.
[15] Weissleder R, Hahn PF, Stark DD, Elizondo G, Saini S, Todd LE, et al. Superparamagnetic iron oxide: enhanced detection of focal splenic tumors with MR imaging. Radiology 1988;169(2):399–403.
[16] Weissleder R, Elizondo G, Wittenberg J, Rabito CA, Bengele HH, Josephson L. Ultrasmall superparamagnetic iron oxide: characterization of a new class of contrast agents for MR imaging. Radiology 1990;175(2):489–93.
[17] Shapiro EM, Skrtic S, Koretsky AP. Sizing it up: cellular MRI using micron-sized iron oxide particles. Magn Reson Med 2005;53(2):329–38.
[18] Metz S, Bonaterra G, Rudelius M, Settles M, Rummeny EJ, Daldrup-Link HE. Capacity of human monocytes to phagocytose approved iron oxide MR contrast agents in vitro. Eur Radiol 2004;14(10):1851–8.
[19] Montet-Abou K, Montet X, Weissleder R, Josephson L. Cell internalization of magnetic nanoparticles using transfection agents. Mol Imaging 2007;6(1):1–9.
[20] Petri-Fink A, Hofmann H. Superparamagnetic iron oxide nanoparticles (SPIONs): from synthesis to in vivo studies – a summary of the synthesis, characterization, in vitro, and in vivo investigations of SPIONs with particular focus on surface and colloidal properties. IEEE Trans Nanobioscience 2007; 6(4):289–97.
[21] Matuszewski L, Persigehl T, Wall A, Schwindt W, Tombach B, Fobker M, et al. Cell tagging with clinically approved iron oxides: feasibility and effect of lipofection, particle size, and surface coating on labeling efficiency. Radiology 2005;235(1):155–61.
[22] Lewin M, Carlesso N, Tung CH, Tang XW, Cory D, Scadden DT, et al. Tat peptide-derivatized magnetic nanoparticles allow in vivo tracking and recovery of progenitor cells. Nat Biotechnol 2000;18(4):410–4.
[23] Arbab AS, Yocum GT, Kalish H, Jordan EK, Anderson SA, Khakoo AY, et al. Efficient magnetic cell labeling with protamine sulfate complexed to ferumoxides for cellular MRI. Blood 2004;104(4):1217–23.
[24] Tai JH, Foster P, Rosales A, Feng B, Hasilo C, Martinez V, et al. Imaging islets labeled with magnetic nanoparticles at 1.5 Tesla. Diabetes 2006;55(11):2931–8.
[25] Walczak P, Kedziorek DA, Gilad AA, Lin S, Bulte JWM. Instant MR labeling of stem cells using magnetoelectroporation. Magn Reson Med 2005;54(4):769–74.
[26] Shapiro EM, Skrtic S, Sharer K, Hill JM, Dunbar CE, Koretsky AP. MRI detection of single particles for cellular imaging. Proc Natl Acad Sci U S A 2004;101(30): 10901–6.
[27] de Vries IJ, Lesterhuis WJ, Barentsz JO, Verdijk P, van Krieken JH, Boerman OC, et al. Magnetic resonance tracking of dendritic cells in melanoma patients for monitoring of cellular therapy. Nat Biotechnol 2005;23(11):1407–13.
[28] Shapiro EM, Medford-Davis LN, Fahmy TM, Dunbar CE, Koretsky AP. Antibody-mediated cell labeling of peripheral T cells with micron-sized iron oxide particles (MPIOs) allows single cell detection by MRI. Contrast Media Mol Imaging 2007;2(3):147–53.
[29] Oude Engberink RD, van der Pol SM, Dopp EA, de Vries HE, Blezer EL. Comparison of SPIO and USPIO for in vitro labeling of human monocytes: MR detection and cell function. Radiology 2007;243(2):467–74.
[30] Foster-Gareau P, Heyn C, Alejski A, Rutt BK. Imaging single mammalian cells with a 1.5 T clinical MRI scanner. Magn Reson Med 2003;49(5):968–71.
[31] Shapiro EM, Sharer K, Skrtic S, Koretsky AP. In vivo detection of single cells by MRI. Magn Reson Med 2006;55(2):242–9.
[32] Song M, Moon WK, Kim Y, Lim D, Song IC, Yoon BW. Labeling efficacy of superparamagnetic iron oxide nanoparticles to human neural stem cells: comparison of ferumoxides, monocrystalline iron oxide, cross-linked iron oxide (CLIO)–NH_2 and tat-CLIO. Korean J Radiol 2007;8(5):365–71.
[33] Shen T, Weissleder R, Papisov M, Bogdanov A, Brady TJ. Monocrystalline iron-oxide nanocompounds (Mion) – physicochemical properties. Magn Reson Med 1993;29(5):599–604.
[34] Pittet MJ, Swirski FK, Reynolds F, Josephson L, Weissleder R. Labeling of immune cells for in vivo imaging using magnetofluorescent nanoparticles. Nat Protoc 2006;1(1):73–9.
[35] Zhao M, Kircher MF, Josephson L, Weissleder R. Differential conjugation of tat peptide to superparamagnetic nanoparticles and its effect on cellular uptake. Bioconjug Chem 2002;13(4):840–4.
[36] Ayyub P, Palkar VR, Chattopadhyay S, Multani M. Effect of crystal size-reduction on lattice symmetry and cooperative properties. Phys Rev B 1995; 51(9):6135–8.
[37] Solomon I. Relaxation processes in a system of two spins. Phys Rev 1955;99:559.
[38] Bloembergen N. Proton relaxation times in paramagnetic solutions. J Chem Phys 1957;27(2):572–3.
[39] Giljohann DA, Seferos DS, Patel PC, Millstone JE, Rosi NL, Mirkin CA. Oligonucleotide loading determines cellular uptake of DNA-modified gold nanoparticles. Nano Lett 2007;7(12):3818–21.
[40] Duncan R, Izzo L. Dendrimer biocompatibility and toxicity. Adv Drug Deliv Rev 2005;57(15):2215–37.
[41] Foged C, Brodin B, Frokjaer S, Sundblad A. Particle size and surface charge affect particle uptake by human dendritic cells in an in vitro model. Int J Pharm 2005;298(2):315–22.
[42] Chung TH, Wu SH, Yao M, Lu CW, Lin YS, Hung Y, et al. The effect of surface charge on the uptake and biological function of mesoporous silica nanoparticles 3T3-L1 cells and human mesenchymal stem cells. Biomaterials 2007; 28(19):2959–66.
[43] Luo D, Saltzman WM. Synthetic DNA delivery systems. Nat Biotechnol 2000; 18(1):33–7.
[44] Shi XY, Wang SH, Sun HP, Baker JR. Improved biocompatibility of surface functionalized dendrimer entrapped gold nanoparticles. Soft Matter 2007; 3(1):71–4.
[45] Malik N, Wiwattanapatapee R, Klopsch R, Lorenz K, Frey H, Weener JW, et al. Dendrimers: relationship between structure and biocompatibility in vitro, and preliminary studies on the biodistribution of I-125-labelled polyamidoamine dendrimers in vivo. 2000;65:133. J Control Release 2000;68(2):299–302.

Please cite this article in press as: Daniel L.J. Thorek, Andrew Tsourkas, Size, charge and concentration dependent uptake of iron oxide particles by non-phagocytic cells, Biomaterials (2008), doi:10.1016/j.biomaterials.2008.05.015